Dalton Transactions

Accepted Manuscript

ROYAL SOCIETY OF CHEMISTRY

www.rsc.org/dalton

Dodecyl Ethyl Dimethyl Ammonium Bromide capped WO_3 nanoparticles: Efficient Scaffold for Chemical Sensing and Environmental Remediation

Sheifali Shukla[1], Savita Chaudhary[1], Ahmad Umar[2,3]*, Ganga Ram Chaudhary[1], S.K. Mehta[1]*

[1]Department of Chemistry and Centre of Advanced Studies in Chemistry, Panjab University, Chandigarh 160 014, India

[2]Department of Chemistry, College of Science and Arts, Najran University, Najran-11001, Kingdom of Saudi Arabia

[3]Promising Centre for Sensors and Electronic Devices (PCSED), Najran University, Najran-11001, Kingdom of Saudi Arabia

[*]**Corresponding authors:**

E-mail: ahmadumar786@gmail.com

E-mail address: skmehta@pu.ac.in

Tel: +91 172 2534423; Fax: +91 172 2545074

Abstract

The current work revealed the comparative analysis of bare and surface functionalized tungsten trioxide (WO_3) nanoparticles that can be successfully utilized as competent photocatalyst for the degradation of organic dye and efficient electron transporter for the fabrication of highly sensitive electrochemical sensors in aqueous medium. The room temperature synthesis of WO_3 nanoparticles with good crystalline nature was carried out in the presence of dodecylethyldimethyl ammonium bromide (DEDMAB) as template by wet chemical process. The surface functionalized nanoparticles possess controllable band gap and act as an effectual substrate for electro chemical sensing of hydrazine. The sensitivity values of the fabricated sensor range from 9.39 μA/μM cm^2 with limits of detection ranging from 28.8μM. Furthermore, surface modulated particles also exhibited enhanced photocatalytic performance for photodegrading Congo red with efficiency of 98.67% as compared to bare WO_3 nanoparticles without any modification. The comparison of current responses and photodegradation activity of bare and capped WO_3 particles illustrates an excellent sensitivity, selectivity and operational stability of as functionalized nanoparticles.

Keywords: Surface functionalized; photocatalyst; electrochemical sensor; Congo red; Hydrazine

1. Introduction

Globally, the rapid industrialization is one of the major causes of ecological injustices, thus, the disproportionate burden either in the form of excessive use of organic chemicals and colouring materials such as dyes is principally one of the major concerns over the years for scientists.[1-4] Azo dyes are used considerably in textile, printing, petrochemicals and other industries.[5,6] On the other hand, Hydrazine and its derivative class of compounds are extensively employed in the fields of agriculture, chemical, pharmaceutical industry, aircrafts, blowing agents, antioxidants, photographic agents, corrosion inhibitors, fuel etc.[7-9] The quantitative discharge of these non-biodegradable, highly toxic, potentially carcinogenic effluents into water bodies and surrounding ecosystem pose a huge threat to environment, inducing multiple human health disorders.[10,11] Keeping in view the detrimental effects on human wellbeing and surrounding ecosystem, effective and dynamic approach for reliable and rational sensing of hydrazine and complete decomposition of organic dyes are highly desired.

Currently, some of the acknowledged biological, chemical and physical treatment procedures including chemical oxidation, activated carbon adsorption, coagulation/flocculation, ultra filtration, microbial degradation, sedimentation, incineration, reverse osmosis, precipitation, and air stripping have been employed for dye removal applications.[12-15] Although spectrophotometric titration, chromatography and fluorescence analysis have been performed for ascertaining the presence of hydrazine or its derivatives in aqueous media,[16,17] however, all these techniques are time-consuming, unreasonably expensive and sample pre-treatments are often required. Hence, search for alternative wastewater treatment techniques focussed the attention towards the use of nanoparticles with large adsorptive surface area, low diffusion resistance, high adsorption capacity, high stability and efficiency.

In this perspective, semiconducting oxide nanoparticles received noteworthy consideration as sensing materials owing to their incredible sensitivity and photocatalytic activity.[18] Out of various metal oxide nanoparticles, n-type semiconductor i.e., tungsten trioxide (WO_3) with wide band gap ranging from 2.4-2.8 eV is one of the most promising materials.[19] WO_3 possess an imperative role in up-coming technologies for ecological remediation. This electrochromic material possesses high stability during irradiation, witnessing strong absorption in the near UV and luminous regions with potential applications in variable-reflectance mirrors, information displays, energy replenishment, energy-saving smart windows and environmental detoxification.[20-22] It is an attractive candidate for an exceptional electrochromic, photochromic and gasochromic material.[23,24]

In the present report, WO_3 nanoparticles with good crystalline nature have been prepared by room temperature wet chemical synthetic process using dodecylethyldimethyl ammonium bromide (DEDMAB) as template. The structural morphologies, optical and thermal properties were characterized by employing TEM, SEM, UV-vis, photoluminescence, FTIR, TGA and XRD analysis. The as functionalized WO_3 nanoparticles were further utilized as competent photo-catalyst for the degradation of Congo red dye. The efficiency of surface functionalized WO_3 was also assessed as electron transporter for highly sensitive electrochemical sensor for hydrazine in aqueous medium. The results were also compared with un-functionalized WO_3 (bare WO_3) particles. The comparison of current responses and photodegradation activity clearly illustrates the super-colossal aptitude of surfactant capped WO_3 NPs over bare nanoparticles for electrochemical sensing and photo gradation activity towards industrial effluents. The method affords a reliable procedure in terms of reproducibility, sensitivity and selectivity.

2. Experimental details

2.1. Material

Dodecylethyldimethyl ammonium bromide (DEDMAB, 99.9%), and Tungsten (VI) chloride (WCl_6, 99.9%) were from Sigma-Aldrich. Sodium dihydrogen phosphate (>99%), disodium hydrogen phosphate (>99%) and ammonia solution (25%, v/v) were purchased from Merck. Acetone (98–100%) and ethanol (99.9%) were obtained from BDH and Changshu Yangyuan (China), respectively. Congo red dye was purchased from SD fine chemicals (CI No 22120). All reagents were used as received without further purification. Double distilled water was used for the solution preparations.

2.2. Synthesis and characterisation of surface functionalized WO_3 nanoparticles

In a usual process, 20ml of 7.0 mM dodecylethyldimethyl ammonium bromide (DEDMAB) solution was equilibrated for 2 h under stirring conditions. 10ml of 0.25 M aqueous ammonia aqueous solution was added to the surfactant mixture to attain hydrolysis. The mixture was continuously stirred for 15 min at 250 rpm to increase homogeneity. After 15 min of aging, 0.9279g of WCl_6 (8.0 mM) was quickly injected into the above mixture with stirring for 1 min, and then the reaction mixture was kept at 30 ℃ under static conditions for 4 h. The subsequent product was aged for 3 days at room temperature and were collected by centrifugation and washed several times with water and ethanol to remove impurities. The obtained material was calcined at 600 $^{\circ}$C for 2 h resulting to generate bare WO_3 NPs for doing comparative analysis.

The diffraction patterns of the surfactant capped and bare WO_3 NPs were recorded by X-ray diffractometer (XRD; PANalytical X'Pert PRO) using with Cu- Kα radiations (λ= 1.54178 Å) in the range of 10–70^0 with $0.02°s^{-1}$. Si ($\Delta 2\theta = 0.06\theta$) was employed as the standard protocol for estimating the instrumental broadening and correction was carried out

by subtracting this value from the Δ2θ values for the samples under investigation. The FTIR spectral data were recorded in a Perkin-Elmer (RX1) FTIR spectrometer, in the range 4400–350 $cm^{-1}$by taking the samples in the form of KBr pellets using standard procedure. The UV−visible absorption spectra were recorded on a JASCO-530V UV-vis spectrophotometer by using a matched pair of quartz cuvette of 1 cm path length in the range of 200 to 1000 nm. The photoluminescence spectra were recorded on Perkin Elmer LS 55 fluorescence spectrophotometer by exciting the sample with 415 nm. Thermal gravimetric analysis (TGA) of the bare nanoparticles as well as DEDMAB was carried out on TGA-DTA instrument SDT Q 600 in the temperature range of 20-1000˚C with the heating rate of 10˚C/min in nitrogen atmosphere using platinum pans. The surface morphology of the samples prepared in aqueous solutions of surfactant was investigated by Hitachi (H-7500) transmission electron microscope operating at 80kV.

3. Results and discussion

3.1. Morphological, Structural and Optical Properties of as-synthesized WO_3 nanoparticles

WO_3 nanoparticles were synthesized by a room temperature wet chemical synthetic process in presence of 12 carbon chained DEDMAB surfactant. In all the syntheses, the molar ratio of the surfactant/ WCl_3/aq. NH_3 was optimized to attain better control over the size of the nanoparticles. Figure 1a presents the XRD patterns of the WO_3 nanoparticles obtained in presence of surfactant and the samples annealed at 600 ˚C for 2 h. The results verified that the XRD peaks of product were indexed to monoclinic structure of WO_3 (JCPDS no 43-1035).[25] The presence of traces of non-stoichiometric compositions was also appeared as the small intensities of peaks at 2θ = 55.1 and 60.8° were also observed which corresponded to WO_2 and metallic tungsten in case of annealed samples. The obtained reflections were sharp and quite intense indicating very good crystallinity of the final product.

The average crystallite sizes calculated from full width at half maxima (FWHM) of diffraction peaks using Debye-Scherrer formula.[26]

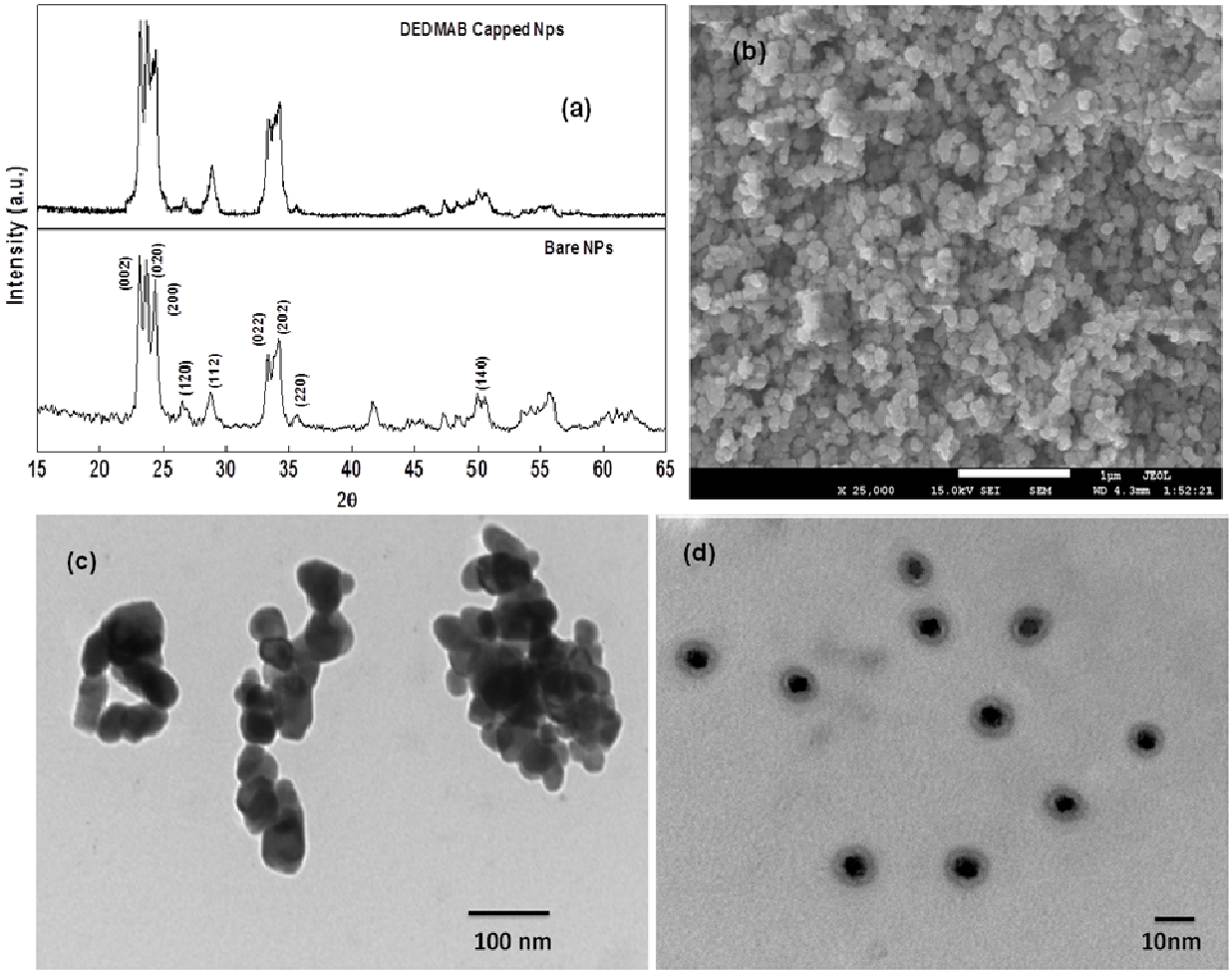

Figure 1. (a) XRD pattern, (b) SEM, (c) TEM of bare and (d) capped WO_3 NPs synthesized from aqueous micellar solution of DEDMAB.

The presence of DEDMAB during the synthesis of WO_3 nanoparticles results in a formation of smaller sized particles with average crystallite size 5.4 nm as compared to the 15 nm WO_3 nanoparticles obtained after calcinations. No difference in the diffraction peak and position was observed in the presence of surfactant i.e. the crystal structure of NPs was not

altered during capping process and surfactant templates never involved in modifying the crystalline structure of the nanoparticles. The main role of capping is to restrict the growth of the particles and modulate the size of the nanoparticles. The effect of surfactant capping on the size of nanoparticles was also assessed by using SEM and TEM analysis (Figure 1b, 1d). The agglomeration rate of surfactant capped nanoparticles is lesser as compared to calcined WO_3 nanoparticles (Figure 1b). The particles are well separated in the presence of surfactant capping, whereas the inter particle interaction was more in the case of calcined samples. The concentration of surfactant also played significant role in stabilizing nanoparticles. At lower concentration, the surface coverage of nanoparticles via surfactant monomers was less and hence the extent of inter-particle interaction among nanoparticles showed significant enhancement as compared to the higher concentration of surfactant. At higher concentrations of DEDMAB, the stabilization occurred via bilayer formation over nanoparticles.

The results were further verified from FTIR analysis of WO_3 nanoparticles. The spectra of pure surfactant, surfactant-capped and bare NPs are shown Fig. 2a. In almost all the cases, a broad peak around 3400-3420 cm^{-1} was observed, attributed to O-H stretching due to some absorbed moisture. For all the surfactants, the conventional bands in the range of 3000-2800 cm^{-1} were due to symmetric and asymmetric $–CH_2$ vibrations of pure surfactants and remained approximately the same in the presence of NPs.[27, 28] This was indicative of the fact that the free alkyl chain of surfactants do not adsorb over the surface of NPs. The peaks around 1560 and 1464 cm^{-1} due to –CH scissoring vibrations of $–N-CH_3$ moiety were either been significantly suppressed or shifted. The peaks at 1067, 940, 920 cm^{-1} due to C-N stretching showed significant variations. The band at 777, 722, 691 cm^{-1}, assignable to ν (W-O-W) group, confirmed the presence of metal-oxygen bonding. [29] A strong stretching vibration around the above said band corresponding to ν (W-O-W) was found. Its existence can be explained on the basis of crystalline structure of WO_3, which is a modified version of

WO_6 octahedra. In this octahedron, the tungsten atoms are placed at the centre and the oxygen atoms are located at the vertices, hence, each oxygen atom is connecting two tungsten atoms. Thus, it was established, the capping of NPs was due to adsorption of surfactant molecules through head groups and that the surfactant molecules degraded to maximum extent as the characteristic peaks of surfactants got disappeared after calcinations. The surface modifications with DEDMAB over nanoparticles also affected the hydrophobic characteristics of nanoparticles and the monomers of surfactants. The thermal decomposition processes for nano-materials and its ingredients were carried out using thermogravimetry (TGA) analysis (Fig. 2b). The initial weight loss of 13.28 % was observed for DEDMAB-capped nanoparticles upto 350 ºC due to physically and chemically bonded water. Further, loss of 27.84 % was mainly due to loss of respective surfactants capping over nanoparticles at 600 ºC.[30] There was no significant change in weight with further heating up to 1000 ˚C showing the phase stability of WO_3 over wide temperature. In case of calcined sample, the total weight loss was found to be hardly 2% showing the importance of surfactants in deciding the stoichiometry and stability of final products. Moreover, an approximately straight line can be observed in the TGA curve of calcined sample, suggesting that it does not possess any hydrate or surfactant residue at all after calcinations.

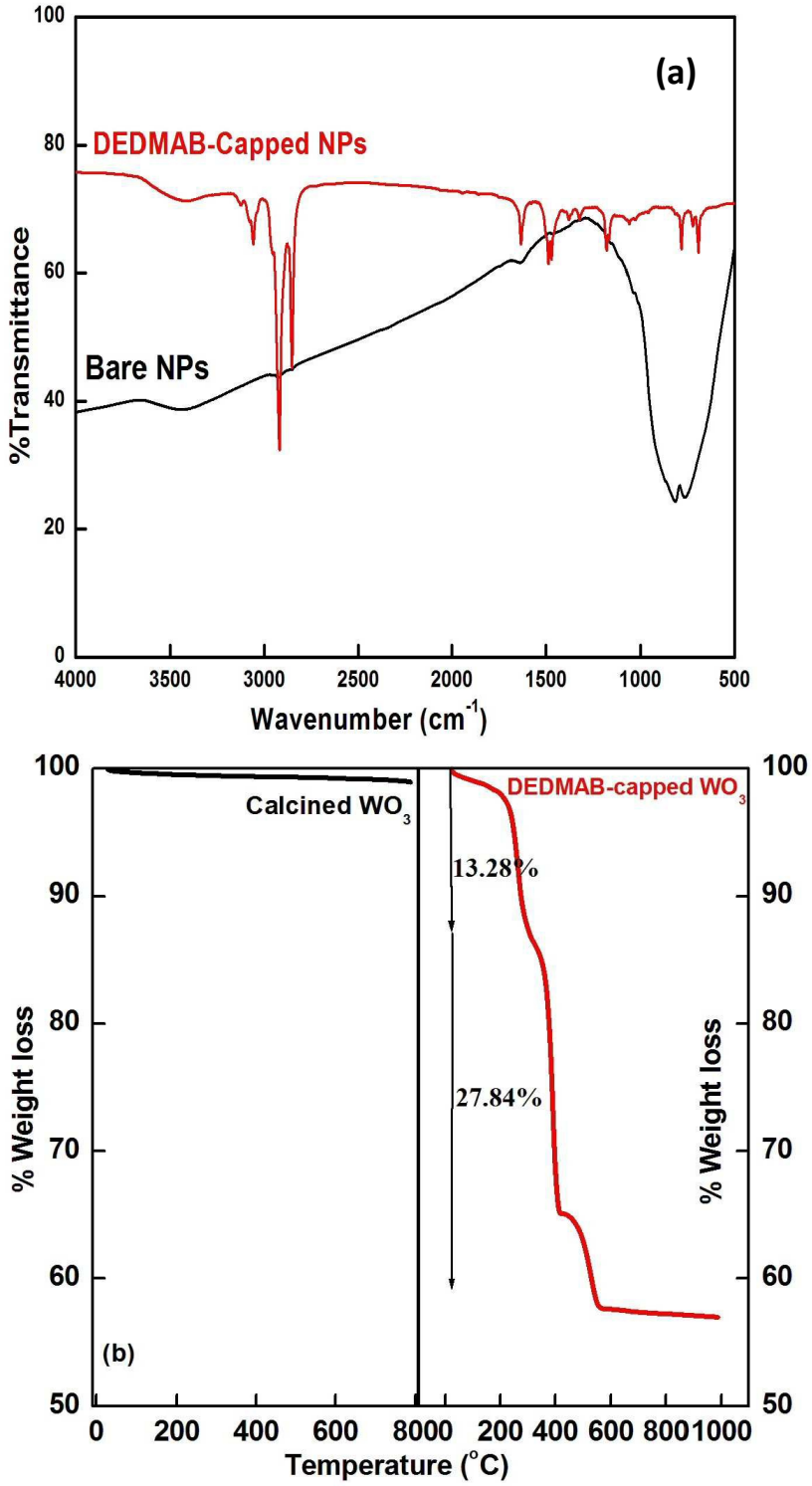

Figure 2. (a) FTIR and (b) TGA spectra of calcined and DEDMAB-capped WO_3 NP's

The room temperature optical absorption and fluorescence spectra were also recorded and the absorption edges along with the band gap values were examined (data not shown here) for surface functionalized WO_3 NPs. Well-defined absorption peak at 320 nm was observed along with the shift of absorption edges towards higher energies. Due to quantum confinement of photo-generated electron-hole pairs, UV-vis absorption spectra turn out to be size dependent. Optical band gap was estimated from the absorbance data by using mentioned below equation.[31]

$$\Delta E_g = \frac{1240}{\lambda}$$

where, ΔEg is the change in the band gap due to quantum confinement and λ is the absorption wavelength. The radius was computed using quantum mechanical calculations for various micellar media using equation:

$$\Delta E_g = \frac{\hbar^2 \pi^2}{2\mu R^2}$$

while the particle agglomeration number was calculated from below equation:

$$n = \frac{4}{3}\pi R^3 \rho N_A M^{-1}$$

where n is the agglomeration number, R is the radius of WO_3 NPs, ρ is the density of the WO_3 (7.16×10^2 kg m^{-3}), N_A is the Avogadro constant, and M is the WO_3 molecular mass. The obtained particle size for WO_3 NPs comes out to be 1.797 nm with agglomeration number equal to 457. These results exhibited consistency with TEM and XRD results.

3.2. Electrocatalytic Activity of surface functionalized WO_3 nanoparticles

The electro-catalytic activity of the surfactant functionalized WO_3 nanoparticles was examined by cyclic voltammetric (CV) technique. Keeping in view of the importance as well as toxicity, analyte i.e., hydrazine was selected for detection and sensing using highly

sensitive, quickly responding and easy-to-handle surfactant functionalized amperometric WO_3–based sensor. The modification of working electrode with higher catalytic active and wide band gap WO_3 NPs helped in lowering the working potential of hydrazine.

3.2.1 Formulation of WO_3-based Electrochemical Sensor for Detection of Hydrazine

To formulate the WO_3-based sensor, the gold electrode (Au; surface area = 3.14 mm^2) was refined with alumina slurry, sonicated in distilled water and dried out at room temperature. The surface of gold electrode was modified using the slurry of butyl carbitol acetate (BCA) and WO_3 NPs (synthesized from aqueous solutions of DEDMAB surfactant). The modified Au electrode was then dried at 60 ± 5 $^{\circ}C$ for 4–6 h to acquire a homogeneous layer over the whole electrode surface. For all the measurements, 0.1 M phosphate buffer (pH 7.0) was used. Electrochemical studies were performed at room temperature using a μAutolab Type-III cyclic voltammeter having three-electrode configuration, i.e. modified gold electrode functioned as working electrode, a Pt wire as a counter electrode and an Ag/AgCl (sat. KCl) as a reference electrode. Figure 3a shows the CV responses of unmodified and modified gold electrode for 1 mM hydrazine in N_2 saturated 0.1 M phosphate buffer (PBS) in the potential scanning range from -0.3 to 0.6V with scan rate of 100 mV s^{-1}. To check the role of nanoparticles in the oxidation of hydrazine, electrode was also modified by using bulk-WO_3. No distinct responses could be monitored in case of bulk WO_3/Au electrode and bare Au electrode in the presence of hydrazine. However, under similar reaction conditions, in the presence of hydrazine, WO_3 Np/Au electrode exhibits a sharp oxidation peak (E_{pa}) with enhanced peak current (I_{pa}) observed at 0.201 V. The considerable changes are associated with the faster electron transportation for WO_3 nanoparticles and act as a good electro-catalyst for the oxidation of hydrazine as compared to bare gold and calcined WO_3 particles (Fig 3). In order to investigate the role of surfactant in electron

transportation, the amplification of current rate was also monitored. The C12 chained surfactant displayed maximum current response of 67.78 µA as compared to C16 chained surfactant (cetylpyridinium bromide CPB).[32] Such variations are associated with the modulation of size and band gap of WO_3 NPs with surfactants. In comparison with higher chain length surfactants, C12 chained DEDMAB has better capping over the nanoparticle surface. The lower agglomeration rate and smaller size provided higher available surface area for WO_3 NPs/Au electrode in electro-catalytic reaction for hydrazine. In addition, the cationic nature of the head group also provides the electrostatic attraction for better peak current response than bare NPs.

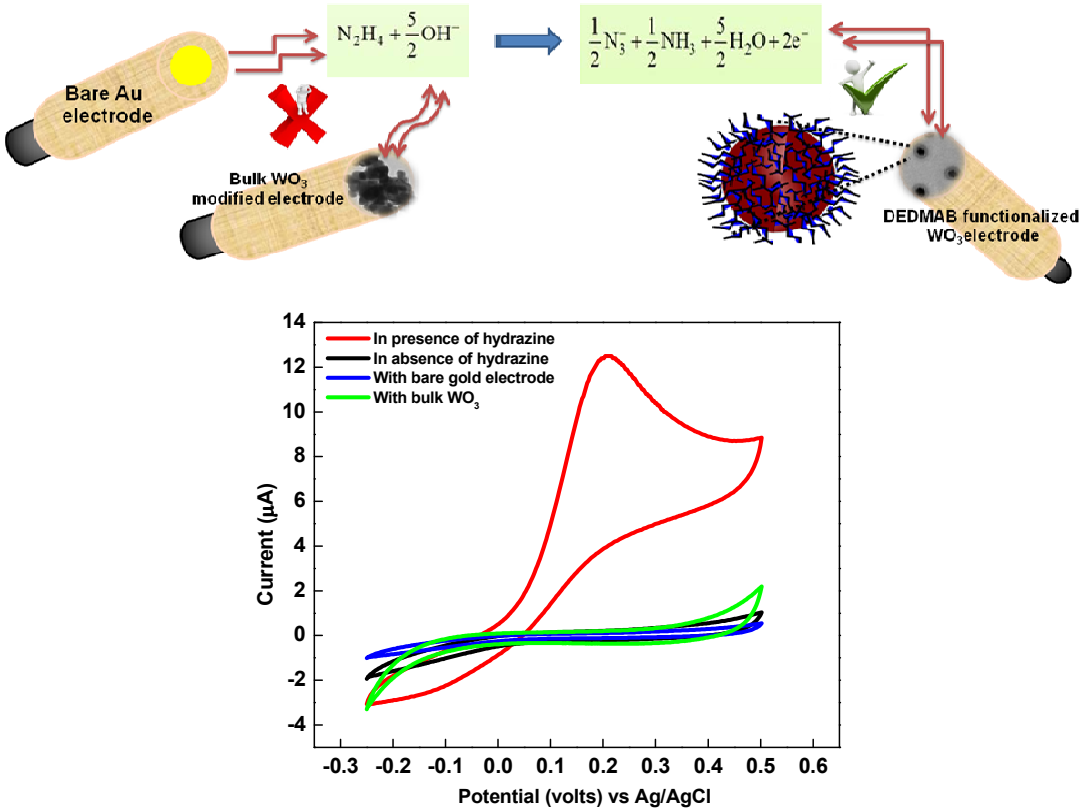

Figure 3. Schemcatic illustration and cyclic voltammetric sweep curves for the WO_3 NPs/Au electrode in the presence and absence of hydrazine, with bare gold electrode and with bulk

WO_3 in 0.1 M phosphate buffer (pH 7.0). The scan rate was 100 mV s^{-1} and hydrazine concentration was kept at 1mM.

The effect of scan rate and concentration of hydrazine was also monitored to understand the mechanism and role of surfactant in electrochemical oxidation of hydrazine (**Fig. 4a, 4b**). The position and magnitude of anodic peak current showed significant variations for bare and DEDMAB capped- WO_3 NPs. Such difference can be explained on the basis of the different dimensional sizes and band gap modulations of WO_3 nanoparticles with DEDMAB.

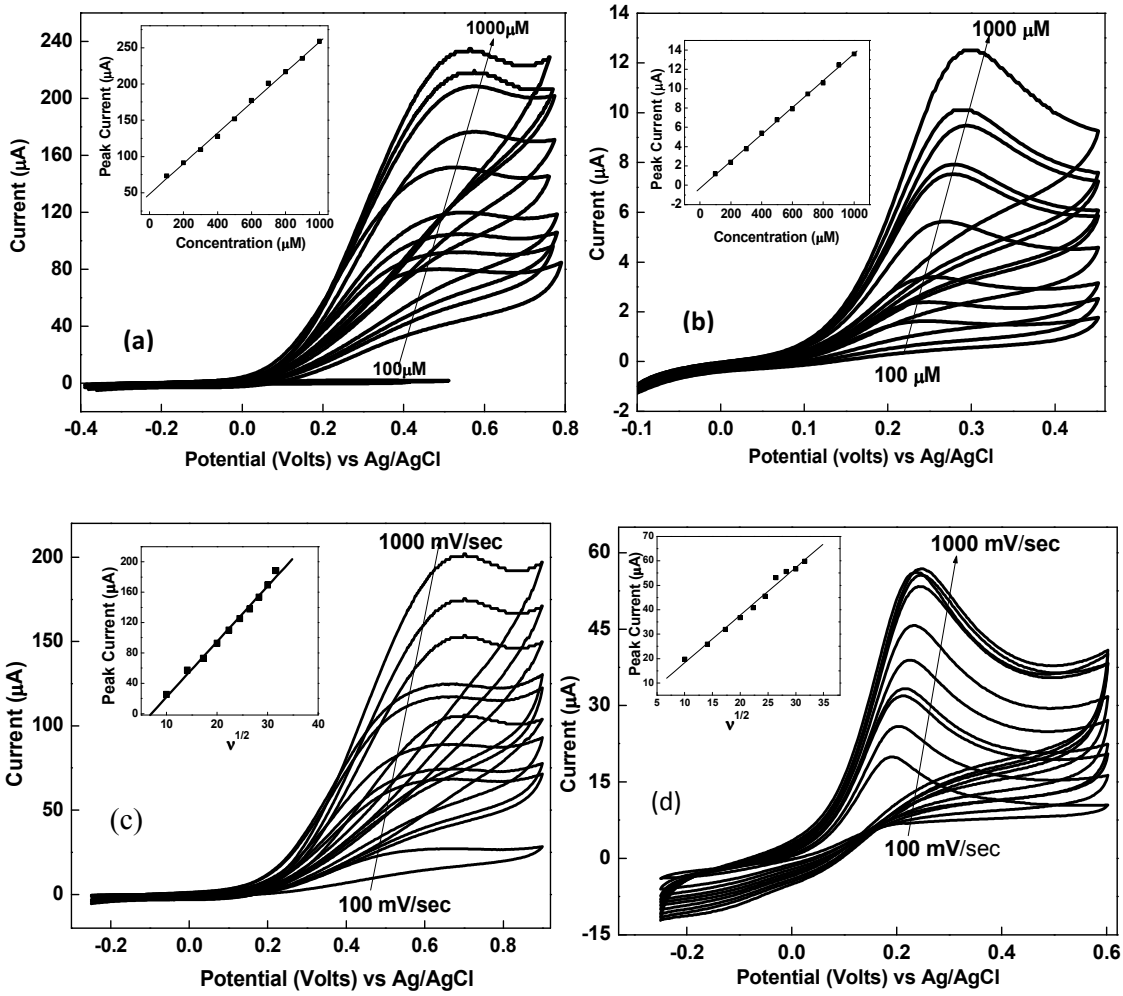

Figure 4. Cyclic voltammograms obtained for 1mM hydrazine in phosphate buffer (7.0) as a function of scan rates (100 to 1000 mV/s) and concentrations (100 to 1000 μM) with DEDMAB functionalized (a,c) and calcined (b,d) WO_3 NPs.

The overall electrons (n) involved in the electrochemical oxidation of hydrazine and nature of electron transfer process were also obtained from the plot of anodic peak current versus square root of scan rate ($\nu^{1/2}$) (Fig 3c inset) for DEDMAB capped WO_3 nanoparticles by using Nicholsan Shain equation.[33]

$$i_p = (2.99x10^5)n(\alpha n_\alpha)^{1/2} ACD^{1/2}\nu^{1/2}$$

where i_p is the peak current density, A is area of electrode (cm^2), C is concentration of electroactive species, D is diffusion constant of electro-active species, υ is scan rate, n is number of electrons exchanged, α is charge transfer coefficient. The corresponding value of αn_α was calculated from following equation:

$$\alpha n_\alpha = \frac{(0.048)}{(E_p - E_{p/2})}$$

where E_p is the peak potential corresponding to i_p and $E_{p/2}$ is half height potential.[34] The sensitivity values of the fabricated sensor range from 9.39 μA/μM cm^2 with limits of detection ranging of 28.8μM.

3.2.2. Amperometric Responses of WO_3-based Electrochemical Sensor for Hydrazine

The sensing efficiency of modified electrodes towards hydrazine was also investigated by amperometric analysis for 100 μM to 1000 μM hydrazine in 0.1 M phosphate buffer (pH 7.0) at a constant potential of 0.35 V (Figure 5a and b). The variations in the peak current response were clearly visualized for calcined and capped-WO_3/Au modified

electrode. The differences were correlated with the different electron transport behaviour of these electrodes in reaction media. The surfactant capping over the nanoparticles surface also enhances the stability as well as the electron transport efficiency of the electrodes. The corresponding shelf life of the electrode was also enhanced with surfactant covering as compared to the bare-WO_3. The fabricated sensor witnessed excellent reproducibility along with tremendous stability and selectivity for some common interfering species like ammonia (NH_3), hydroxylamine (NH_2OH), nitrate ion (NO^{3-}), nitrite ion (NO^{2-}) monitored at fixed potential with WO_3/Au-electrode (Fig. 6).

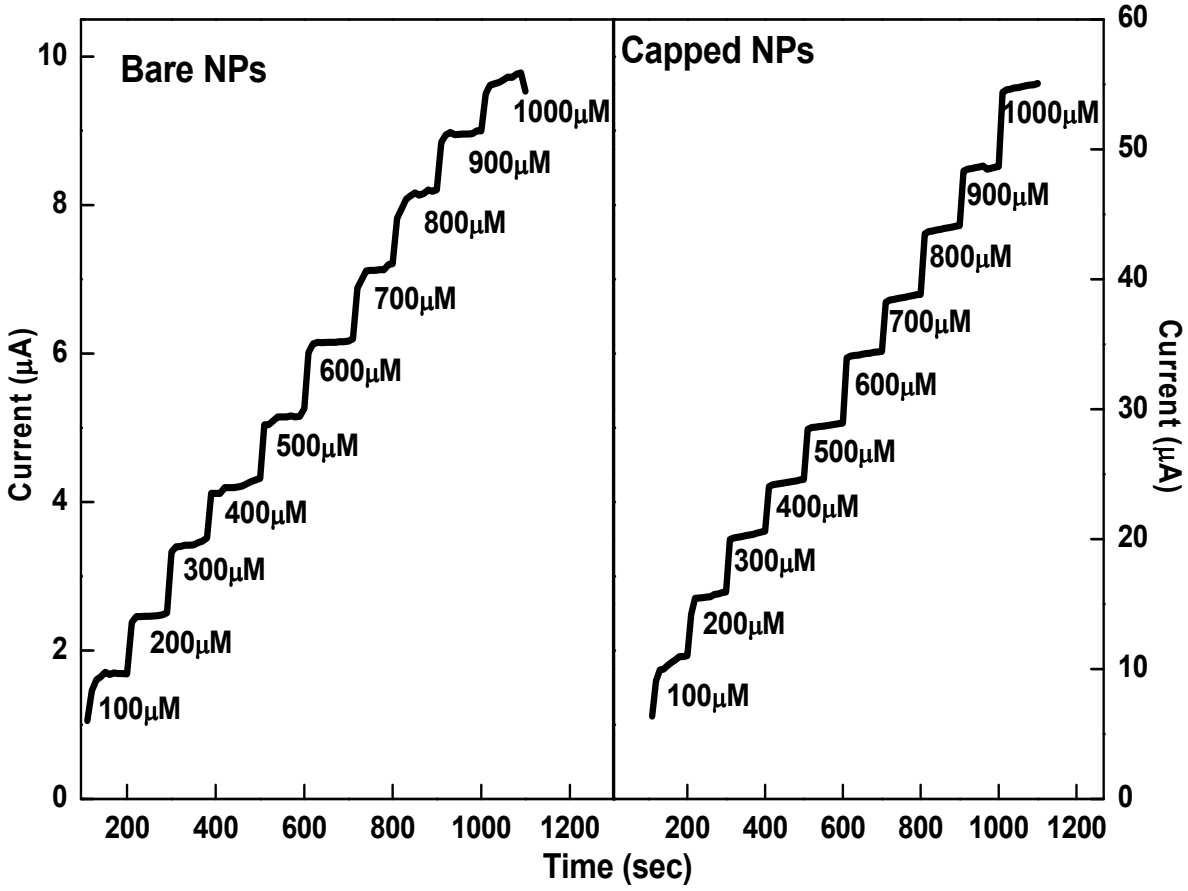

Figure 5. Amperometric response obtained for 1mM hydrazine in phosphate buffer (7.0) with bare) and capped WO_3 NPs synthesized in aqueous micellar solution of DEDMAB.

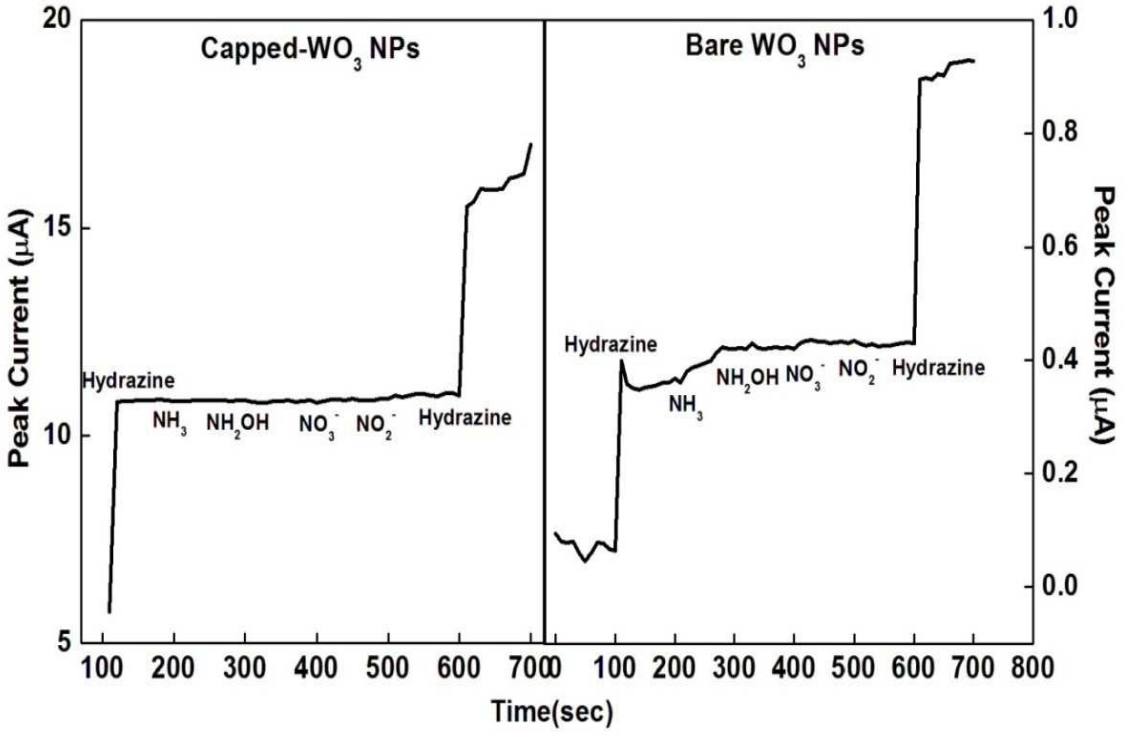

Figure 6. Amperometric response of bare-WO_3/Au electrode and capped-WO_3/Au electrode in the presence of various interfering ions/compounds

3.3. Evaluation of Photocatalytic Activity of surface functionalized WO_3 nanoparticles

The photocatalytically active, surfactant-functionalized WO_3 NPs were further employed for photodegradation of the carcinogenic anionic azo dye, i.e, congo red. The reaction was carried out in double-walled 250 ml quartz reactor into which long Teflon tube was inserted. 125 W UV high pressure mercury lamp was employed for irradiation of solution. The intensity of the lamp was >198.4 μW/cm^2. The temperature of the reaction solution was maintained using thermostat. 25 mg of photocatalyst was added to 100 ml (25 mg/l) aqueous solution of Congo red dye. The source was kept 35 cm above the surface of the solution. The pH was maintained at 5.5. The solution was magnetically stirred throughout the experiment to ensure uniform dispersion of photocatalyst. Prior to irradiation, the solution

was stirred in dark for 1 hour to attain adsorption-desorption equilibrium between photocatalyst and organic dye substrates. After, switching on the UV source, the aliquots were collected at different time intervals for a total of 60 minutes. The samples were then filtered using 0.45μm millipore syringe filters and the absorbance spectra of all the samples were recorded. The degradation of dye was examined in terms of change in intensity and percent degradation was evaluated as:

$$\frac{C_o - C}{C_o} \text{ x } 100$$

where, C_o is the initial concentration of dye and C is the concentration at time t. The characteristic peak of pure dye at 497 nm and 352 nm showed significant decrease in the absorbance after adding surfactant functionalized nanoparticles of WO_3 as compared to calcined WO_3 particles within 5 minutes of UV exposure (Figure 7a). The analysis was also done in dark and in the presence of light for comparing the results. There was no degradation in dark for surfactant functionalized or calcined WO_3 particles. On the other hand 90.70% dye was degraded in the presence of UV light for surfactant functionalized particles as compared to 15% degradation for calcined nanoparticles. The percentage variation changes enormously as the concentration of more and more dosage amount of DEDMAB functionalized particles were added to the reaction system (Figure 7b) keeping the dye concentration fixed at 25mg/L. The degradation efficiencies were seen to be linearly dependent on the dosage amount of the catalyst from 50 to 250 mg/L. On further enhancing the dosage amount, no noticeable increase in degradation efficiency was observed. This behavioural aspect could be explained on the basis of increased number of active sites on the surface of catalyst on increasing the catalyst dose. The increased amount of photocatalyst led to absorption of increased number of photons which induced direct augmentation in number of active radical species that are readily accessible for degradation of dye. However, on

raising the catalyst dose above 250 mg/L causes agglomeration which results in reduction in the total active surface area available for adsorption of dye.

In order to ensure the effect of surfactant on degradation, similar analysis was also carried out for DEDMAB alone (Fig 7a). Interestingly in this case no degradation of dye was observed (Fig 7a). Therefore, degradation efficiency was only dependent on the surface functionalization of NPs which simply assisted the photocatalytic activity of nanoparticles, firstly, by providing positive surface due to cationic headgroups, thus attracting the anionic dye molecules over NP surface and secondly, by restricting the crystallite size which enhanced the surface area to volume ratio of photocatalysts, thereby increasing the number of reactive sites (Figure 7c). The dye removal efficiency and kinetics of the WO_3 nanoparticles in DEDMAB micellar media were also corroborated with the time-dependent absorption spectra. The linear kinetic plots between 1/C vs. t suggest that photodegradation followed the second order kinetics. The kinetic parameters such as rate constants, k and linear regression coefficients, R^2 were evaluated from linear plots of 1/C vs. t (Fig 7b inset).

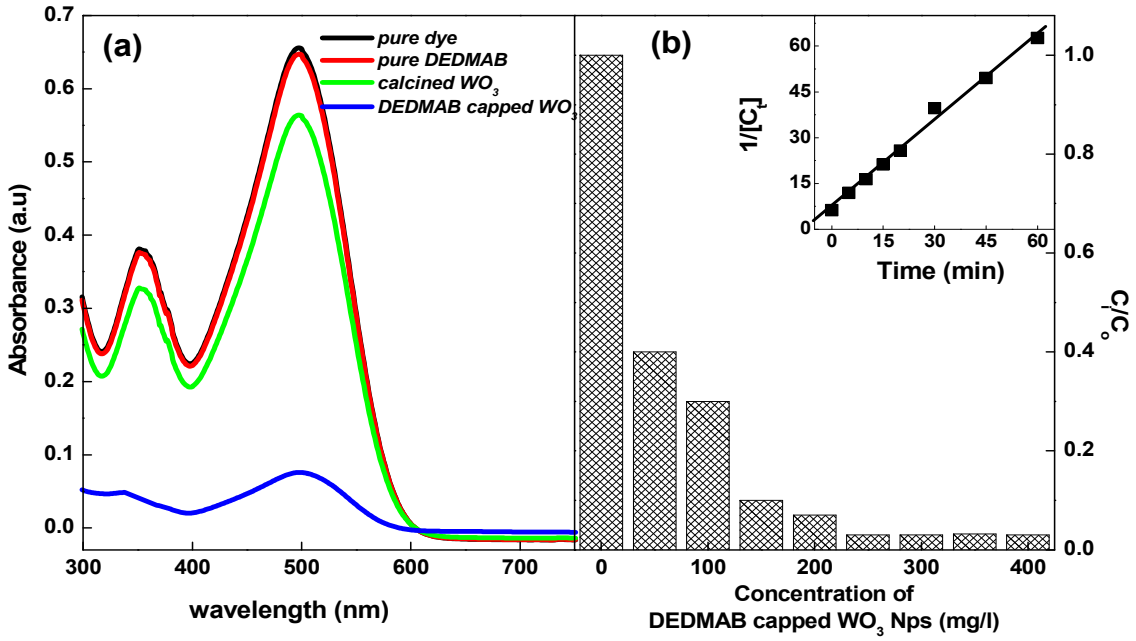

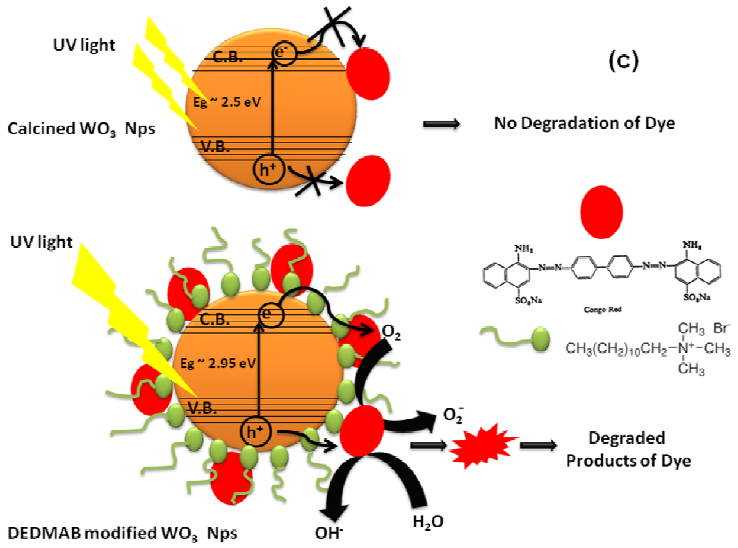

Figure 7 (a) Degradation of dye in the presence pure surfactant, capped WO_3 NPs and bare WO_3 NPs. (b) Effect of catalyst concentration on degradation efficiency of dye. Inset Kinetic analysis of photodegradation of Congo red dye in presence of DEDMAB functionalized WO_3 nanoparticles. (c) Pictorial representation of mechanism of dye degradation using surface functionalized WO_3 nanoparticles.

The extent of capping of DEDMAB significantly influenced the crystallite size of the nanoparticles which in return increased the surface area, number of reactive sites and surface hydroxyl groups over the exterior surface of nanoparticles. The recombination rate of electrons and holes was further reduced by the capping of DEDMAB and more e^-/h^+ are generated and transferred to the exterior surface of WO_3 and subsequently enhance degradation rate as compared to calcined nanoparticles (Figure 7c). The recyclability of the catalyst was also carried out by collecting the NPs from sample solution after centrifugation and proper washing. The degradation efficiency of recycled sample was found to be comparable with freshly prepared samples after four uses. The results verified the excellent chemical stability and practical utility of WO_3 nanoparticles in DEDMAB micellar media.

4. Conclusions

In summary, well-crystalline monoclinic, high-yield WO_3 nanostructures were synthesized and characterized maintaining the stability and stoichiometry in micellar media of DEDMAB at room temperature conditions. The simply-synthesized WO_3 NPs were used as efficient electron mediators for construction of amperometric hydrazine electrochemical sensor with higher selectivity, stability and reproducibility. The modified sensor displayed a broader exponential response for hydrazine recognition upto 900 μM. The sensitivity of the obtained sensor was about 9.39 μA/μM cm^2 with limits of detection ranging to 28.8μM. Furthermore, surfactant functionalized particles were employed for photocatalytic degradation of Congo red dye with efficiency as high as of 98.67% as compared to bare WO_3 nanoparticles without any modification. The comparison of current responses and photodegradation activity of bare and capped WO_3 particles illustrates an excellent sensitivity, selectivity and operational stability of as functionalized nanoparticles. The present report opens up the feasibility of using functionalised WO_3 NPs as potential photocatalysts and electrochemical sensor for effective decontamination of environment pollutants.

Acknowledgments

Authors are thankful to DST for Purse grant. Savita Chaudhary is grateful to DST Inspire Faculty award [IFA-CH-17] and UGC Start up Grant with reference number 20-1/2011(BSR) for financial assistance. Sheifali Shukla is thankful to UGC for financial assistance. S.K. Mehta is thankful to SERB DST for major research project. Ahmad Umar would like to thank Ministry of Higher Education, Saudi Arabia for granting Promising Centre for Sensors and Electronic Devices at Najran University, Saudi Arabia.

References

[1] (a) I.K. Konstantinou, T.A. Albanis, *Appl. Catal. B: Environ*. 2004, **49**, 1–14; (b) A. Li, J. Liu, S. Feng, *Sci. Adv. Mater.* 2014, 6, 209-234; (c) J. H. Kim, J. S. Lee, *Energy Environ. Focus* 2014, **3**, 339-353; (d) S. Liu, G. Wang, Y. Li, L. Meng, *Sci. Adv. Mater.* 2014, **6**, 361-365

[2] (a) W.X. Yin, Z.P. Li, J.K. Zhu, H.Y. Qi, *J. Power Sources* 2008, **182**, 520-523; (b) P. Jing, W. Lan, Q. Su, M. Yu, E. Xie, *Sci. Adv. Mater.* 2014, **6**, 434-440; (c) D. Hou, W. Zhou, X. Liu, K. Zhou, G. Li, S. Chen, *Energy Environ. Focus* 2014, **3**, 330-338; (d) W. Zhou, D. Wang, H. Liu, J. Wang, *Sci. Adv. Mater.* 2014, **6**, 538-544

[3] (a) S.D. Zelnick, D.R. Mattie, P.C. Stepaniak , *Aviat. Space Environ. Med.* 2003, **74**, 1285-1291; (b) L.-Y. Chen, W.-D. Zhang, *Sci. Adv. Mater*. 2014, **6**, 1091-1098; (c) L. Chu, M. Li, P. Cui, Y. Jiang, Z. Wan, S. Dou, *Energy Environ. Focus* 2014, **3**, 371-374; (d) S. Zhang, R. Wang, S. Zhang, G. Li, Y. Zhang, *Sci. Adv. Mater*. 2014, **6**, 1262-1268

[4] E.H. Vernot, J.D. MacEwen, R.H. Bruner, C.C. Haus, E.R. Kinkead, *Fundam. Appl. Toxicol.*1985, **5,** 1050-1064; (b) L. Tian, C. Gong, J. Liu, L.Ye, L. Zan, *Sci. Adv. Mater.* 2013, **5**, 1627-1632; (c) C. Chen, H. Chen, J. Shi, J. Yu, *Sci. Adv. Mater.* 2014, **5**, 896-903

[5] M. Ahmad, E. Ahmed, Z.L. Hong, N.R. Khalid, W. Ahmed, A. Elhissi, *J. Alloys Compd.*2013, **577,** 717–727.

[6] K. Melghit, M.S. Al-Rubaei, I. Al-Amri, *J. Photochem. Photobiol. A* 2006, **181,** 137–141.

[7] A. Savafi, M.A. Karimi, *Talanta* 2002, **58,** 785-792.

[8] A. Safavi, A.A. Ensafi, *Anal. Chim. Acta* 1995, **300**, 307-311.

[9] G.E. Collins, S.L. Rose-Pehrsson, *Anal. Chim. Acta.* 1993, **284**, 207-215.

[10] I. Arslan, I.A. Balcioglu, T. Tuhkanen, D. Bahnemann, *J. Environ. Eng*. 2000, **126** 903–911.

[11] S.K. Chaudhuri, B. Sur, *J. Environ. Eng.* 2000, **126,** 583–594.

[12] S. Khorramfar, N.M. Mahmoodi, M. Arami, H. Bahrami, *Desalination* 2011, **279**, 183–189.

[13] M.S.U. Rehman, M. Munir, M. Ashfaq, N. Rashid, M.F. Nazar, M. Danish, *Chem. Eng. J.* 2013, **228**, 54–62.

[14] M.C. Wei, K.S. Wang, C.L. Huang, C.W. Chiang, T.J. Chang, S.S. Lee, *Chem. Eng. J.* 2012, **192**, 37–44.

[15] S. Barredo-Damas, M.I. Alcaina-Miranda, M.I. Iborra-Clar, J.A. Mendoza-Roca, *Chem. Eng. J.* 2012, **192**, 211–218.

[16] H.J. Zhang, J.S. Huang, H.Q. Hou, T.Y. You, *Electroanalysis* 2009, **21**, 1869-1874.

[17] L. Zheng, J.F. Song, *Talanta* 2009, **79**, 319-326.

[18] C.G. Kuo, C.Y. Chou, Y.C. Tung, J.H. Chen, *J. Marine Sci. Tech*. 2012, **20**, 365-368.

[19] M. Hepel, H. Redmond, I. Dela, *Electrochim. Acta.* 2007, **52**, 3541-3549.

[20] J.H. Ha, P. Muralidharan, D.K. Kim, *J. Alloys Compd.* 2009, **475**, 446-451.

[21] F. Amano, M. Tian, G. Wu, B. Ohtani, A.J. Chen, *Solid State Electrochem*. 2012, **16**, 1965-1973.

[22] D. Meng, T. Yamazaki, Y. Shen, Z. Liu, T. Kikuta, *Appl. Surf. Sci*. 2009, **25**, 1050-1053.

[23] W. Wu, Y. Qingkai, J. Lian, B. Jiming, L. Zhihong, P. Shin-Shem, *J. Cryst. Growth* 2010, **312**, 3147-3150.

[24] A. Mahshad, M. Ali Reza, R. Alimorad, *Iran J. Chem. Eng*. 2012, **31**, 23-29.

[25] H. Yan, X .Zhang, S. Zhou, X. Zhie, Y. Luo, Y. You, *J. Alloys Comp*. 2011, **509**, L232-L235

[26] A.A. Ismail, *Appl. Catal. B: Environ.* 2008, **85**, 33-39.

[27] J. Luo, M. Hepel, *Electrochim. Acta* 2001, **46**, 2913–2922.

[28] K. Hayat, M.A. Gondal, M.M. Khaled, Z.H. Yamani, S. Ahmed, *J. Hazard. Mater*. 2011, **186**, 1226–1233.

[29] V.B. Kumar, D. Mohanta, *Bull. Mater. Sci* 2011, **34**, 435-442.

[30] Mahshad, M.A. Reza, R. Alimorad, Iran. *J. Chem. Chem. Eng* 2012, **31**, 23-29.

[31] M. Hepel, J. Luo, *Electrochim. Acta* 2001, **47**, 729–740.

[32] S. Shukla, S. Chaudhary, A. Umar, G.R. Chaudhary, S.K. Mehta, *Sens. Actuators, B* 2014, **196**, 231–237.

[33] R.S. Nicholsan, I. Shain, *Anal. Chem.* 1964, **36**, 706-723.

[34] A. Ensafi, H.K. Maleh, *Int. J. Electrochem. Sci.* 2010, **5**, 1484-1495.